
Learning Hierarchical Priors in VAEs

Alexej Klushyn^{1,2} Nutan Chen¹ Richard Kurlle^{1,2} Botond Cseke¹ Patrick van der Smagt¹

¹Machine Learning Research Lab, Volkswagen Group, Munich, BY, Germany

²Department of Informatics, Technical University of Munich, Munich, BY, Germany

{a.klushyn, botond.cseke}@argmax.ai

Abstract

We propose to learn a hierarchical prior in the context of variational autoencoders. Our aim is to avoid over-regularisation resulting from a simplistic prior like a standard normal distribution. To incentivise an informative latent representation of the data by learning a rich hierarchical prior, we formulate the objective function as the Lagrangian of a constrained-optimisation problem and propose an optimisation algorithm inspired by Taming VAEs. To validate our approach, we train our model on the static and binary MNIST, Fashion-MNIST, OMNIGLOT, CMU Graphics Lab Motion Capture, 3D Faces, and 3D Chairs datasets, obtaining results that are comparable to state-of-the-art. Furthermore, we introduce a graph-based interpolation method to show that the topology of the learned latent representation correspond to the topology of the data manifold.

1. Introduction

Variational autoencoders (VAEs) (Kingma & Welling, 2013; Rezende et al., 2014) are a class of latent variable models for unsupervised learning. The learned generative model and the corresponding (approximate) posterior distribution of the latent variables provide a decoder/encoder pair that might capture semantically meaningful features of the data. In this paper, we address the issue of learning informative latent encodings/representations of the data.

The vanilla VAE uses a standard normal prior distribution for the latent variables. However, it has been shown that this often leads to over-regularising the posterior distribution, resulting in a poor latent representation (Alemi et al., 2018). There are several approaches to alleviate this problem: (i) defining and learning complex prior distributions that can model the encoded data manifold (Chen et al., 2016b; Tomczak & Welling, 2018); (ii) using specialised optimisation algorithms that try to find local minima of the

training objective that correspond to informative latent representations (Bowman et al., 2016; Sønderby et al., 2016; Higgins et al., 2017; Rezende & Viola, 2018); and (iii) adding mutual-information based constraints or regularisers to incentivise a good correspondence between the data and the latent variables (Alemi et al., 2018; Zhao et al., 2017; Chen et al., 2016a). In this paper, we address the first two approaches.

As a starting point, we use the approach from (Tomczak & Welling, 2018), where the authors note that the optimal prior (empirical Bayes) is the aggregated posterior—a uniform mixture of approximate posteriors evaluated at the data points. Using this insight, they propose a prior that is a uniform mixture of approximate posterior distributions, evaluated at a few learned pseudo data points. However, a finite mixture does not always provide a good prior (e.g., Sec. 4.2). In this paper, we propose to approximate the aggregated posterior through a continuous mixture/hierarchical distribution. This enables a highly flexible prior, and hence avoids over-regularising the approximate posterior.

In order to learn such hierarchical priors, we extend the optimisation framework, introduced in (Rezende & Viola, 2018), where the authors reformulate the VAE objective as the Lagrangian of a constrained-optimisation problem. They impose the reconstruction error as inequality constraint and choose the KL divergence between the approximate posterior and the prior as the optimisation objective. Instead of a standard normal, we use the hierarchical distribution described above as prior and approximate it by applying an importance-weighted bound (Burda et al., 2015). Concurrently, we introduce the associated optimisation algorithm, inspired by GECO (Rezende & Viola, 2018), since the latter does not always lead to good encodings (e.g., Sec. 4.1). Our approach prevents posterior collapse and results in more informative latent representations than previous methods.

We adopt the manifold hypothesis (Cayton, 2005; Rifai et al., 2011) to validate the quality of a latent representation. We do this by proposing a nearest-neighbour graph-based method for interpolating between different data points along the learned data manifold in the latent space.

2. Methods

2.1. VAEs as a Constrained-Optimisation Problem

VAEs model the distribution of i.i.d. data $\mathcal{D} = \{\mathbf{x}_i\}_{i=1}^N$ as the marginal

$$\prod_i p_\theta(\mathbf{x}_i) = \prod_i \int p_\theta(\mathbf{x}_i|\mathbf{z}) p(\mathbf{z}) d\mathbf{z}. \quad (1)$$

The model parameters are learned through amortised variational EM, which requires learning an approximate posterior distribution $q_\phi(\mathbf{z}|\mathbf{x}_i) \approx p_\theta(\mathbf{z}|\mathbf{x}_i)$. It is hoped that the learned $q_\phi(\mathbf{z}|\mathbf{x})$ and $p_\theta(\mathbf{x}|\mathbf{z})$ result in an informative latent representation of the data. For example, $\{\mathbb{E}_{q_\theta(\mathbf{z}|\mathbf{x}_i)}[\mathbf{z}]\}_{i=1}^N$ cluster w.r.t. some discrete features or important factors of variation in the data. In Sec. 4.1, we show a toy example, where the model can learn the true underlying factors of variation in \mathcal{D} .

Amortised variational EM in VAEs maximises the evidence lower bound (ELBO) (Kingma & Welling, 2013; Rezende et al., 2014):

$$\begin{aligned} \mathbb{E}_{p_{\mathcal{D}}(\mathbf{x})} [\log p_\theta(\mathbf{x})] &\geq \mathcal{F}_{\text{ELBO}}(\theta, \phi) \\ &\equiv \mathbb{E}_{p_{\mathcal{D}}(\mathbf{x})} \left[\mathbb{E}_{q_\phi(\mathbf{z}|\mathbf{x})} [\log p_\theta(\mathbf{x}|\mathbf{z})] - \mathbb{KL}(q_\phi(\mathbf{z}|\mathbf{x})\|p(\mathbf{z})) \right], \quad (2) \end{aligned}$$

where $q_\phi(\mathbf{z}|\mathbf{x})$ and $p_\theta(\mathbf{x}|\mathbf{z})$ are typically assumed to be diagonal Gaussians and their parameters are defined as neural network functions of the conditioning variables. $p_{\mathcal{D}}(\mathbf{x}) = \frac{1}{N} \sum_{i=1}^N \delta(\mathbf{x} - \mathbf{x}_i)$ stands for the empirical distribution of the data \mathcal{D} . The (EM) optimisation problem (e.g. Neal & Hinton, 1998) is formulated as

$$\min_{\theta, \phi} -\mathcal{F}_{\text{ELBO}}(\theta, \phi) \hat{=} \min_{\theta} \min_{\phi} -\mathcal{F}_{\text{ELBO}}(\theta, \phi). \quad (3)$$

The corresponding optimisation algorithm has been often implemented as a double loop algorithm, however, in the context of VAEs—or neural inference models in general—it is a common practice to optimise (θ, ϕ) jointly.

It has been shown that local minima with high ELBO values do not necessarily result in informative latent representations (Alemi et al., 2018; Higgins et al., 2017). In order to address this problem, several approaches have been developed, which typically result in some weighting schedule for either the negative expected log-likelihood or the KL term of the ELBO (Bowman et al., 2016; Sønderby et al., 2016). This is due to the fact that a different ratio targets different regions in the rate-distortion plane, either favouring better compression or reconstruction (Alemi et al., 2018).

In (Rezende & Viola, 2018), the authors reformulate the VAE objective as the Lagrangian of a constrained-optimisation problem. They choose the $\mathbb{KL}(q_\phi(\mathbf{z}|\mathbf{x})\|p(\mathbf{z}))$ as the optimisation objective and impose the inequality constraint $\mathbb{E}_{p_{\mathcal{D}}(\mathbf{x})} \mathbb{E}_{q_\phi(\mathbf{z}|\mathbf{x})} [C_\theta(\mathbf{x}, \mathbf{z})] \leq \kappa^2$. Typically

$C_\theta(\mathbf{x}, \mathbf{z})$ is defined as the reconstruction-error-related term in $-\log p_\theta(\mathbf{x}|\mathbf{z})$. Since $\mathbb{E}_{p_{\mathcal{D}}(\mathbf{x})} \mathbb{E}_{q_\phi(\mathbf{z}|\mathbf{x})} [C_\theta(\mathbf{x}, \mathbf{z})]$ is the average reconstruction error, this formulation allows for a better control of the quality of generated data. In the resulting Lagrangian objective

$$\begin{aligned} \mathcal{L}(\theta, \phi; \lambda) &\equiv \mathbb{E}_{p_{\mathcal{D}}(\mathbf{x})} \left[\mathbb{KL}(q_\phi(\mathbf{z}|\mathbf{x})\|p(\mathbf{z})) \dots \right. \\ &\quad \left. + \lambda (\mathbb{E}_{q_\phi(\mathbf{z}|\mathbf{x})} [C_\theta(\mathbf{x}, \mathbf{z})] - \kappa^2) \right], \quad (4) \end{aligned}$$

the Lagrange multiplier λ can be viewed as a weighting term for $\mathbb{E}_{p_{\mathcal{D}}(\mathbf{x})} \mathbb{E}_{q_\phi(\mathbf{z}|\mathbf{x})} [\log p_\theta(\mathbf{x}|\mathbf{z})]$. This approach leads to a similar optimisation objective as in (Higgins et al., 2017) with $\beta = 1/\lambda$. The authors propose a descent-ascent algorithm (GECO) for finding the saddle point of the Lagrangian. The parameters (θ, ϕ) are optimised through gradient descent and λ is updated as

$$\lambda_t = \lambda_{t-1} \cdot \exp(\nu \cdot (\hat{C}_t - \kappa^2)), \quad (5)$$

corresponding to a quasi-gradient ascent due to $\Delta\lambda_t \cdot \partial_\lambda \mathcal{L} \geq 0$; ν is the update learning rate. In the context of stochastic batch gradient training, $\hat{C}_t \approx \mathbb{E}_{p_{\mathcal{D}}(\mathbf{x})} \mathbb{E}_{q_\phi(\mathbf{z}|\mathbf{x})} [C_\theta(\mathbf{x}, \mathbf{z})]$ is estimated as the running-average $\hat{C}_t = (1 - \alpha) \cdot \hat{C}_{\text{ba}} + \alpha \cdot \hat{C}_{t-1}$, where \hat{C}_{ba} is the batch average $\mathbb{E}_{p_{\mathcal{D}}(\mathbf{x}_{\text{ba}})} \mathbb{E}_{q_\phi(\mathbf{z}|\mathbf{x})} [C_\theta(\mathbf{x}, \mathbf{z})]$. To the best of our understanding¹, the GECO algorithm solves the optimisation problem

$$\min_{\theta} \max_{\lambda} \min_{\phi} \mathcal{L}(\theta, \phi; \lambda) \quad \text{s.t.} \quad \lambda > 0. \quad (6)$$

Here, $\max_{\lambda} \min_{\phi} \mathcal{L}(\theta, \phi; \lambda)$ can be viewed to correspond to the E-step of the EM algorithm. However, in general this objective can only be guaranteed to be the ELBO if $\lambda = 1$, or in case of $0 < \lambda < 1$, a lower bound on the ELBO.

2.2. Hierarchical Priors for Learning Informative Latent Representations

In this section, we propose a hierarchical prior for VAEs within the constrained-optimisation setting. Our goal is to incentivise the learning of informative latent representations and to avoid over-regularising the posterior distribution (i) by increasing the complexity of the prior distribution $p(\mathbf{z})$, and (ii) by providing an optimisation method to learn such models.

It has been shown that the optimal empirical Bayes prior is the aggregated posterior distribution

$$p^*(\mathbf{z}) = \mathbb{E}_{p_{\mathcal{D}}(\mathbf{x})} [q_\phi(\mathbf{z}|\mathbf{x})]. \quad (7)$$

We follow (Tomczak & Welling, 2018) to approximate this distribution in the form of a mixture distribution. However,

¹The optimisation problem is not explicitly stated in (Rezende & Viola, 2018).

we opt for a continuous mixture/hierarchical model

$$p_{\Theta}(\mathbf{z}) = \int p_{\Theta}(\mathbf{z}|\zeta) p(\zeta) d\zeta, \quad (8)$$

with a standard normal $p(\zeta)$. This leads to a hierarchical model with two stochastic layers. As a result, intuitively, our approach inherently favours the learning of continuous latent features. We refer to this model by variational-hierarchical prior (VHP).

In order to learn the parameters in Eq. (8), we propose to adapt the constrained-optimisation problem in Sec. 2.1 to hierarchical models. For this purpose we use an importance-weighted (IW) bound (Burda et al., 2015) to create a sequence of upper bounds (and constrained-optimisation problems). That is, we use

$$\begin{aligned} \mathbb{E}_{p_{\mathcal{D}}(\mathbf{x})} \mathbb{KL}(q_{\phi}(\mathbf{z}|\mathbf{x}) \| p(\mathbf{z})) &\leq \mathcal{F}(\phi, \Theta, \Phi) \\ &\equiv \mathbb{E}_{p_{\mathcal{D}}(\mathbf{x})} \mathbb{E}_{q_{\phi}(\mathbf{z}|\mathbf{x})} \left[\log q_{\phi}(\mathbf{z}|\mathbf{x}) \dots \right. \\ &\quad \left. - \mathbb{E}_{\zeta_{1:K} \sim q_{\Phi}(\zeta|\mathbf{z})} \left[\log \frac{1}{K} \sum_{k=1}^K \frac{p_{\Theta}(\mathbf{z}|\zeta_k) p(\zeta_k)}{q_{\Phi}(\zeta_k|\mathbf{z})} \right] \right], \quad (9) \end{aligned}$$

with K importance weights, defining an upper bound on Eq. (4):

$$\begin{aligned} \mathcal{L}(\theta, \phi; \lambda) &\leq \mathcal{F}(\phi, \Theta, \Phi) + \lambda (\mathbb{E}_{p_{\mathcal{D}}(\mathbf{x})} \mathbb{E}_{q_{\phi}(\mathbf{z}|\mathbf{x})} [\mathcal{C}_{\theta}(\mathbf{x}, \mathbf{z})] - \kappa^2) \\ &\equiv \mathcal{L}_{\text{VHP}}(\theta, \phi, \Theta, \Phi; \lambda). \quad (10) \end{aligned}$$

As a result, we arrive to the optimisation problem

$$\min_{\Theta, \Phi} \min_{\theta} \max_{\lambda} \min_{\phi} \mathcal{L}_{\text{VHP}}(\theta, \phi, \Theta, \Phi; \lambda) \quad \text{s.t.} \quad \lambda > 0, \quad (11)$$

which we can optimise by the following double loop algorithm: (i) in the *outer loop* we update the bound w.r.t. (Θ, Φ) ; (ii) in the *inner loop* we solve the optimisation problem $\min_{\theta} \max_{\lambda} \min_{\phi} \mathcal{L}_{\text{VHP}}(\theta, \phi, \Theta, \Phi; \lambda)$ by applying an update scheme for λ and $\beta = 1/\lambda$, respectively. In the following, we use the β -parameterisation to be in line with (Higgins et al., 2017; Sønderby et al., 2016, e.g.).

In the GECO update scheme (Eq. (5)), β increases/decreases until $\hat{C}_t = \kappa^2$. However, provided the constraint is fulfilled, we want to obtain a lower bound on the log-likelihood. As discussed in Sec. 2.1, that can be guaranteed when $\beta = 1$ (ELBO). To achieve this, we propose to replace the corresponding β -version of Eq. (5) by

$$\beta_t = \beta_{t-1} \cdot \exp[\nu \cdot f_{\beta}(\beta_{t-1}, \hat{C}_t - \kappa^2; \tau) \cdot (\hat{C}_t - \kappa^2)], \quad (12)$$

where we define

$$f_{\beta}(\beta, \delta; \tau) = (1 - H(\delta)) \cdot \tanh(\tau \cdot (\beta - 1)) - H(\delta). \quad (13)$$

Here, $H(\cdot)$ is the Heaviside function and we introduce a slope parameter τ . This update can be interpreted as follows.

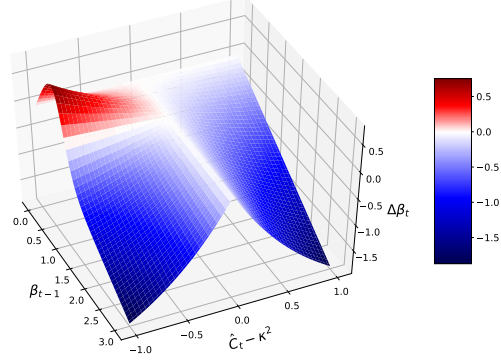


Figure 1. β -update scheme: $\Delta\beta_t = \beta_t - \beta_{t-1}$ as a function of β_{t-1} and $\hat{C}_t - \kappa^2$ for $\nu = 1$ and $\tau = 3$. A comparison with the GECO update scheme can be found in App. A. (see Sec. 2.2)

If the constraint is violated, i.e. $\hat{C}_t > \kappa^2$, the update scheme is equal to Eq. (5) due to the Heaviside function. In case the constraint is fulfilled, the tanh term guarantees that we finish at $\beta = 1$, to obtain/optimize the ELBO at the end of the training. Thus, we impose $\beta \in (0, 1]$, which is reasonable since $\beta < \beta_{\max}$ does not violate the constraint. A visualisation of the β -update scheme is shown in Fig. 1.

However, the double loop approach in Eq. (11) is often computationally inefficient. Thus, we decided to run the inner loop only until the constraints are satisfied and then updating the bound. That is, we optimise Eq. (11) and skip the outer loop/bound updates when the constraints are not satisfied. It turned out that the bound updates were often skipped in the initial phase, but rarely skipped later on. Hence, the algorithm behaves as layer-wise pre-training algorithm (Bengio et al., 2007). For these reasons, we propose Alg. 1 (REWO) that separates training into two phases: an initial phase, where we only optimise the reconstruction error and a main phase, where we update all parameters jointly.

In the initial phase, we initialise $\beta \ll 1$ to enforce a reconstruction optimisation. Thus, to train the first stochastic layer for achieving a good encoding of the data through $q_{\phi}(\mathbf{z}|\mathbf{x})$, measured by the reconstruction error. For preventing β to become smaller than the initial value during the first iteration steps, we start to update β when the condition $\hat{C}_t < \kappa^2$ is fulfilled. A good encoding is required to learn the conditionals $q_{\Phi}(\zeta|\mathbf{z})$ and $p_{\Theta}(\mathbf{z}|\zeta)$ in the second stochastic layer. Otherwise, $q_{\Phi}(\zeta|\mathbf{z})$ would be strongly regularised towards $p(\zeta)$, resulting in $\mathbb{KL}(q_{\Phi}(\zeta_i|\mathbf{z}) \| p(\zeta_i)) \approx 0$, from which it typically does not recover (Sønderby et al., 2016). In the main phase, after $\hat{C}_t < \kappa^2$ is fulfilled, we additionally optimise the parameters of the second stochastic layer and start to update β . This approach avoids posterior collapse in both stochastic layers (see Sec. 4.1 and App. D.2), and thereby supports the hierarchical prior to learn an informative latent representation for preventing the aforementioned over-regularisation.

Algorithm 1 (REWO) Reconstruction-error-based weighting of the objective function

```

Initialise  $t = 1$ 
Initialise  $\beta \ll 1$ 
Initialise INITIALPHASE = TRUE
while training do
    Read current data batch  $\mathbf{x}_{\text{ba}}$ 
    Sample from variational posterior  $\mathbf{z} \sim q_{\phi}(\mathbf{z}|\mathbf{x}_{\text{ba}})$ 
    Compute  $\hat{\mathbf{C}}_{\text{ba}}$  (batch average)
     $\hat{\mathbf{C}}_t = (1 - \alpha) \cdot \hat{\mathbf{C}}_{\text{ba}} + \alpha \cdot \hat{\mathbf{C}}_{t-1}$ , ( $\hat{\mathbf{C}}_0 = \hat{\mathbf{C}}_{\text{ba}}$ )
    if  $\hat{\mathbf{C}}_t < \kappa^2$  then
        INITIALPHASE = FALSE
    end if
    if INITIALPHASE then
        Optimise  $\mathcal{L}_{\text{VHP}}(\theta, \phi, \Theta, \Phi; \beta)$  w.r.t  $\theta, \phi$ 
    else
         $\beta \leftarrow \beta \cdot \exp[\nu \cdot f_{\beta}(\beta_{t-1}, \hat{\mathbf{C}}_t - \kappa^2; \tau) \cdot (\hat{\mathbf{C}}_t - \kappa^2)]$ 
        Optimise  $\mathcal{L}_{\text{VHP}}(\theta, \phi, \Theta, \Phi; \beta)$  w.r.t  $\theta, \phi, \Theta, \Phi$ 
    end if
     $t \leftarrow t + 1$ 
end while
    
```

The proposed method, which is a combination of an ELBO-like Lagrangian and an IW bound, can be interpreted as follows: the posterior of the first stochastic layer $q_{\phi}(\mathbf{z}|\mathbf{x})$ can learn an informative latent representation due to the flexible hierarchical prior. Since a diagonal Gaussian $q_{\Phi}(\zeta|\mathbf{z})$ is not flexible enough to capture the (true) posterior of the second stochastic layer, we propose to enhance it by using an importance-weighted bound (Cremer et al., 2017) (alternatively, one could use, for example, normalising flows (Rezende & Mohamed, 2015)). This has the following advantages: (i) it facilitates learning a precise conditional $p_{\Theta}(\mathbf{z}|\zeta)$ from the standard normal distribution $p(\zeta)$ to the aggregated posterior $\mathbb{E}_{p_{\mathcal{D}}(\mathbf{x})}[q_{\phi}(\mathbf{z}|\mathbf{x})]$; (ii) it allows $q_{\phi}(\mathbf{z}|\mathbf{x})$ to fully exploit its representational capacity—otherwise, the model could compensate a less expressive $q_{\Phi}(\zeta|\mathbf{z})$ by regularising $q_{\phi}(\mathbf{z}|\mathbf{x})$ (see App. B.3).

2.3. Graph-Based Interpolations for Verifying Latent Representations

A key reason for introducing hierarchical priors was to facilitate an informative latent representation due to less over-regularisation of the posterior. To verify the quality of the latent representations, we build on the manifold hypothesis, defined in (Cayton, 2005; Rifai et al., 2011). The idea can be summarised by the following assumption: real-world data presented in high-dimensional spaces is likely to concentrate in the vicinity of nonlinear sub-manifolds of much lower dimensionality. Following this hypothesis, the quality of latent representations can be evaluated by interpolating between different data points along the learned data man-

ifold in the latent space—and reconstructing the resulting path to the observable space.

To realise the above idea, we propose a graph-based method (Chen et al., 2018) which summarises the continuous latent space by a graph consisting of a finite number of nodes. The nodes $\mathbf{Z} = \{\mathbf{z}_1, \dots, \mathbf{z}_N\}$ can be obtained by randomly sampling N samples from the learned prior (Eq. (8)):

$$\mathbf{z}_n, \zeta_n \sim p_{\Theta}(\mathbf{z}|\zeta)p(\zeta), \quad n = 1, \dots, N. \quad (14)$$

The graph is henceforth constructed by connecting each of them by undirected edges to its k -nearest neighbours. The edge weights are Euclidean distances in the latent space between the related node pairs. Once the graph is built, interpolation between data points \mathbf{x}_i and \mathbf{x}_j can be done as follows. First, we encode the data points as $\mathbf{z}_{(\cdot)} = \mu_{\theta}(\mathbf{x}_{(\cdot)})$, where $\mu_{\theta}(\mathbf{x}_{(\cdot)})$ is the mean of $q_{\phi}(\mathbf{z}|\mathbf{x}_{(\cdot)})$. Next, the encoded data is added as new nodes to the graph along with edges to the existing (nearest neighbour) nodes.

To find the shortest path through the graph between nodes \mathbf{z}_i and \mathbf{z}_j , a classic search algorithm such as A^* can be used. The result is a sequence $\mathbf{Z}_{\text{path}} = (\mathbf{z}_i, \mathbf{z}_{\text{sub}}, \mathbf{z}_j)$, where $\mathbf{Z}_{\text{sub}} \subseteq \mathbf{Z}$, representing the shortest path in the latent space along the learned latent manifold. Finally, to obtain the interpolation we reconstruct \mathbf{Z}_{path} to the observable space.

3. Related Work

Several works improve the VAE by learning more complex priors such as the stick-breaking prior (Nalisnick & Smyth, 2017), a nested Chinese Restaurant Process prior (Goyal et al., 2017), Gaussian mixture priors (Dilokthanakul et al., 2016), or autoregressive priors (Chen et al., 2016b). A closely related line of research is based on the insight that the optimal prior is the aggregated posterior. The VampPrior (Tomczak & Welling, 2018) approximates the aggregated posterior by a uniform mixture of approximate posterior distributions, evaluated at a few learned pseudo data points. In our approach, the aggregated posterior is approximated by using an IW bound. Compared to the VampPrior, the VHP can be viewed as a continuous mixture distribution.

In the context of VAEs, hierarchical latent variable models were already introduced earlier (Rezende et al., 2014; Burda et al., 2015; Sønderby et al., 2016). Compared to our approach, these works have in common the structure of the generative model but differ in the factorisation of the inference models and the optimisation procedure. In our proposed method, the VAE objective is reformulated as the Lagrangian of a constrained-optimisation problem. The prior of this ELBO-like Lagrangian is approximated by an IW bound. It is motivated by the fact that a single stochastic layer with a flexible prior is sufficient for modelling an informative latent representation. The second stochastic layer

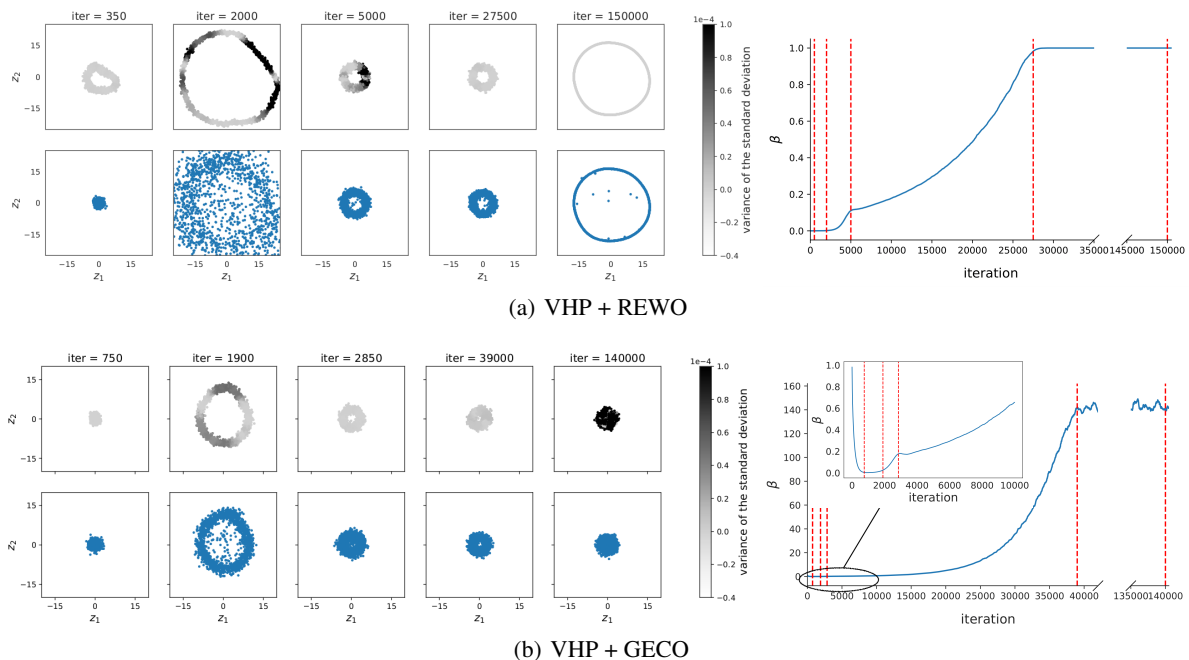


Figure 2. (left) Latent representation of the pendulum data at different iteration steps when optimising $\mathcal{L}_{\text{VHP}}(\theta, \phi, \Theta, \Phi; \beta)$. The top row shows the approximate posterior; the greyscale encodes the variance of its standard deviation. The bottom row shows the hierarchical prior. (right) β as a function of the iteration steps; red lines mark the iteration steps, where the latent representation is visualised. (see Sec. 4.1)

is required to learn a sufficiently flexible prior. Building on that, we provide a detailed interpretation how different stochastic layers in hierarchical models interact—showing us how to tackle optimisation difficulties, and therefore better utilise the model’s capacity.

The common problem of failing to use the full capacity of the model in VAEs (Burda et al., 2015) has been addressed by applying *annealing/warm-up*, where the KL divergence between the approximate posterior and the prior is multiplied by a weighting factor (Bowman et al., 2016; Sønderby et al., 2016). It changes by a predefined schedule, e.g. linearly from 0 to 1. However, such predefined schedules might be suboptimal. Therefore, (Rezende & Viola, 2018) introduce a constrained-optimisation algorithm called GECCO. By reformulating the objective as a constrained-optimisation problem, the above weighting term can be represented by a Lagrange multiplier and updated based on the reconstruction error. Our proposed algorithm builds on GECCO, providing several modifications discussed in Sec. 2.2.

(Higgins et al., 2017) proposed a constant factor, as a hyperparameter, to scale the KL divergence. Instead of the ELBO, they choose a heuristic cost to maximise a measure of latent disentanglement. In contrast to our approach, the goal is not to learn a latent representation that reflects the topology of the data but a disentangled representation, where different dimensions of the latent space represent different features of the data.

4. Experiments

To validate our approach, we conducted the following experiments. In Sec. 4.1, we provide an overview of our approach on toy data consisting of pendulum images. In Sec. 4.2, we consider real-world data (CMU Graphics Lab Motion Capture Database), where we use a low-dimensional latent dimension for visualisation purposes. In Sec. 4.3, we evaluate the log marginal likelihood on standard datasets such as MNIST, Fashion-MNIST, and OMNIGLOT. In Sec. 4.4, we qualitatively evaluate the latent representations of high-dimensional image data of 3D Faces and 3D Chairs by using our graph-based interpolation. The model architectures can be found in App. F.

4.1. Artificial Pendulum Dataset

We created a dataset of 15,000 images of a moving pendulum (see Fig. 4). Each image has a size of 16×16 pixels and the joint angles are distributed uniformly in the range $[0, 2\pi)$. This joint angle is the only degree of freedom.

Fig. 2 shows latent representations of the pendulum data learned by the VHP applying REWO and GECCO, respectively; the same κ is used in both cases. In case of REWO, the approximate posterior $q_\phi(\mathbf{z}|\mathbf{x})$ (Fig. 2(a), top row) is optimised to reach a low reconstruction error at the beginning of the training due to $\beta \ll 1$. The variance of the posterior’s standard deviation, expressed by the greyscale, measures whether the contribution to the ELBO is equally distributed

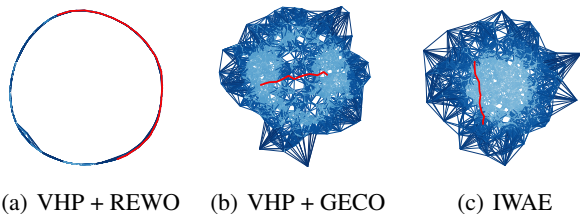


Figure 3. The graphs base on the learned latent encodings of the pendulum data shown in Fig. 18. The red curves depict the interpolation along the resulting data manifold. The blue lines in the graph indicate the edge weights. (see Sec. 4.1)

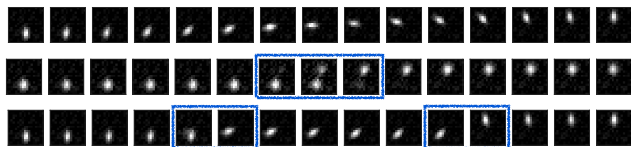


Figure 4. (top row: VHP + REWO, middle row: VHP + GECO, bottom row: IWAE) Pendulum reconstructions of the graph-based interpolation in Fig. 3. Discontinuities are marked by blue boxes. (see Sec. 4.1)

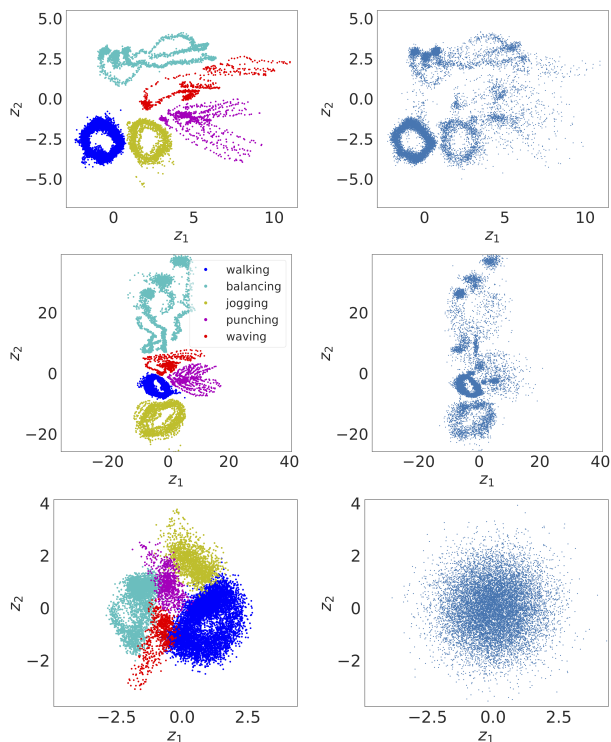


Figure 5. Latent representation of human motion data: VHP + REWO (top), VampPrior (middle), and IWAE (bottom); approximate posterior (left) and prior (right). The colour encodes the five human motions. The different sample densities are caused by a different amount of data points for each motion. (see Sec. 4.2)

over all data points. Once $\hat{C}_t < \kappa^2$ is fulfilled (Fig. 2(a), iter=350), β begins to be updated and the parameters of the second stochastic layer (Θ, Φ) start to be optimised, leading to informative hierarchical prior distributions (Fig. 2(a), bottom row). Between iteration 2000 and 5000, the increase in β results in a regularisation of the latent representation, and hence in a higher reconstruction error. At iteration 5000, β stops to increase due to $\hat{C}_t \approx \kappa^2$ (see Eq. (12)). From iteration 5000 to 27,500, β is updated driven by an interplay between the reconstruction error and the KL divergence, $\hat{C}_t \approx \kappa^2$. After $\beta = 1$, the regularisation impact of the KL divergence does not increase anymore, leading to an improvement of the latent representation (Fig. 2(a), iter=150,000).

To validate whether the obtained latent representation is informative, we apply a linear regression after transforming the latent space to polar coordinates. The goal is to predict the joint angle of the pendulum. We compare REWO with the GECO, and additionally with *warm-up* (WU) (Sønderby et al., 2016), a linear annealing schedule of β . In the latter, we use a VAE objective—defined as an ELBO/IW bound combination, similar to Eq. (10); the related results are in App. B.1. Tab. 1 shows the absolute errors (OLS regression) for the different optimisation procedures; details on the regression can be found in App. B.2. REWO leads to the most precise prediction of the ground truth.

Table 1. Absolute errors of the OLS regressions in Fig. 15 on the learned latent representations of the pendulum data.

METHOD	ABSOLUTE ERROR
VHP + REWO	0.054
VHP + GECO	0.53
VHP*	0.49
VHP* + WU (20 EPOCHS)	0.20
VHP* + WU (200 EPOCHS)	0.31

*VAE OBJECTIVE

Furthermore, we demonstrate that a less expressive posterior $q_\Phi(\zeta|\mathbf{z})$ in the second stochastic layer leads to poor latent representations, since the model compensates it by restricting $q_\phi(\mathbf{z}|\mathbf{x})$, as discussed in Sec. 2.2 (see App. B.3).

We compare the latent representations learned by the VHP and IWAE using the graph-based interpolation method. The graphs, shown in Fig. 3, are built (see Sec. 2.3) based on 1000 samples from the prior of the respective model. The red curves depict the interpolation along resulting data manifold, between pendulum images with joint angles of 0 and 180 degrees, respectively. The reconstructions of the interpolations are shown in (Fig. 4). The top row (VHP + REWO) shows a smooth change of the joint angles, whereas the middle (VHP + GECO) and bottom row (IWAE) contain discontinuities resulting in a less realistic interpolation.

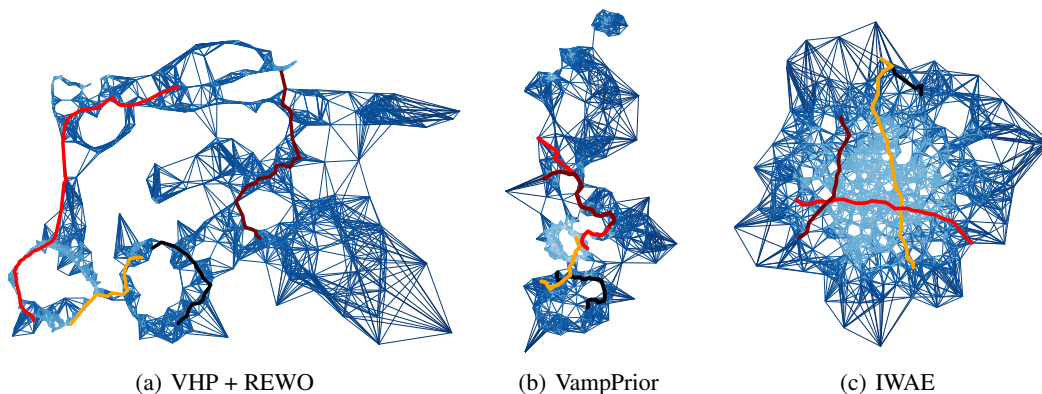


Figure 6. Graph-based interpolation of human motions corresponding to the learned priors in Fig. 5. The blue colour indicates the distance between two nodes. The coloured lines represent four interpolated movements, which can be found in Fig. 7 and App. C. (see Sec. 4.2)

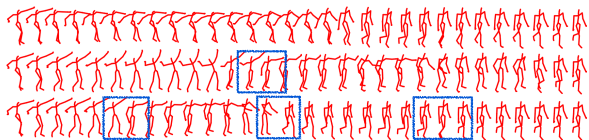


Figure 7. Human movement interpolation for VHP + REWO (top), VampPrior (middle) and IWAE (bottom). Discontinuities are marked by blue boxes. The movement corresponds to the red curve in Fig. 6. (see Sec. 4.2)

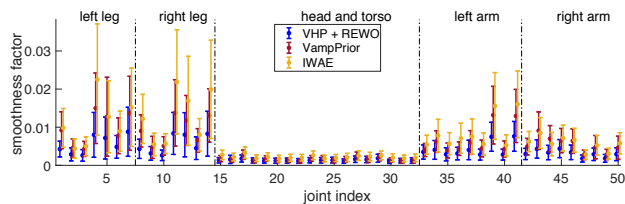


Figure 8. Smoothness measure of human movement interpolations. For each joint, the mean and standard deviation of the smoothness factor are displayed. Smaller values correspond to smoother movements. (see Sec. 4.2)

4.2. Human Motion Capture Database

This section presents the evaluation on the CMU Graphics Lab Motion Capture Database², which consists of several human motion recordings. Our experiments are based on data of five different motions. Since different motions have similar body positions in certain frames, the corresponding manifolds are connected, making it a suitable dataset for interpolation experiments. After preprocessing, each frame is represented by a 50-dimensional feature vector. Due to the low dimensionality of the processed data, we use a two-dimensional latent space that is easy to visualise. The training and validation datasets consist of 12,653 and 2,531 frames, respectively. The VHP, VampPrior, and IWAE have

²<http://mocap.cs.cmu.edu/>

the same architecture for those parts, which the models have in common. The VampPrior is trained with 64 pseudo inputs and the IWAE uses 32 importance samples.

The prior and aggregated approximate posterior of the three methods is shown in Fig. 5. As expected, for both the VHP and VampPrior the latent representations of different movements are separated. In both cases the learned prior matches the aggregated posterior. By contrast, the IWAE is restricted by the Gaussian prior and cannot represent the different motions separately in the latent space. Next, we generate four interpolations (Fig. 6) using our graph-based approach. For this purpose, we interpolate between two frames within one motion (black line) and between two frames of different motions (orange, red, and maroon), visualised in Fig. 7 and App. C. The VampPrior and the VHP lead to smooth interpolations, whereas the IWAE interpolations show abrupt changes in the movements.

Fig. 8 depicts the movement smoothness factor, which we define as the RMS of the second order finite difference along the interpolated path. Thus, smaller values correspond to smoother movements. For each of the three methods, it is averaged across 10 graphs and 100 interpolations for each graph. The 100 starting and ending points are randomly selected. The results show that the latent representation learned by the VHP leads to smoother movement interpolations than in case of the VampPrior and IWAE.

4.3. Evaluation on MNIST, Fashion-MNIST, and OMNIGLOT

We compare our method to the VampPrior and IWAE on MNIST (Lecun et al., 1998), Fashion-MNIST (Xiao et al., 2017), and OMNIGLOT (Lake et al., 2015). We evaluate our method quantitatively by reporting the marginal log-likelihood (LL) on the test set. For MNIST, we report the LL for both dynamic and the static binarisation of (Larochelle & Murray, 2011). Following the test protocol of previous

work (Tomczak & Welling, 2018), we evaluate the LL using importance sampling with 5,000 samples (Burda et al., 2015). Model and training details can be found in App. F. The results are reported in Tab. 2.

VHP + REWO performs as good or better than state of the art on these datasets. The same κ was used for training VHP with REWO and GEKO. The two stochastic layer hierarchical IWAE does not perform better than VHP + REWO, supporting our claim that a flexible prior in the first stochastic layer and a flexible approximate posterior in the second stochastic layer is sufficient. Additionally, we show that REWO leads to a similar amount of active units as WU (200 epochs). Results can be found in App. D.2.

Table 2. Negative test log-likelihood estimated with 5,000 importance samples.

	DYNAMIC MNIST	STATIC MNIST	FASHION- MNIST	OMNI- GLOT
VHP + REWO	78.88	82.74	225.37	101.78
VHP + GEKO	95.01	96.32	234.73	108.97
VAMPRIOR	80.42	84.02	232.78	101.97
IWAE (L=1)	81.36	84.46	226.83	101.57
IWAE (L=2)	80.66	82.83	225.39	101.83

4.4. Qualitative Results: 3D Chairs and 3D Faces

In this section, we evaluate the learned representations qualitatively on 3D Faces (Paysan et al., 2009) and 3D Chairs (Aubry et al., 2014) by using our graph-based interpolation. We generated the Faces dataset with images of 2000 faces with 37 views each. The Chairs dataset consists of 1393 chair images with 62 views each.

Both the VHP + REWO and the IWAE are trained using a 32-dimensional latent space. Fig. 9(a) and 10(a) show interpolations along the latent manifold learned by the VHP + REWO. Compared to the IWAE (Fig. 9(b) and 10(b)), they are less blurry and smoother. Further results can be found in App. E.

5. Conclusion

We proposed the combination of a reconstruction-error-based optimisation procedure and a hierarchical prior, in the context of variational autoencoders, for learning an informative latent representation.

In Sec. 4, we showed that the learned hierarchical prior is indeed non-trivial, moreover, it is well-adapted to the latent representation, reflecting the topology of the encoded data manifold. We observe that for dynamic data, as in case of the pendulum (Sec. 4.1), REWO facilitates the model to learn a sufficiently informative latent representation—allowing to predict the pendulum’s angle by a simple OLS

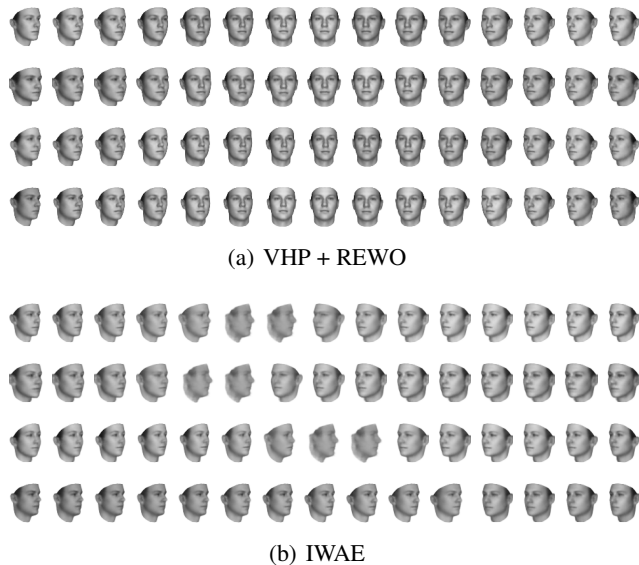


Figure 9. Faces: interpolations along the learned latent manifold with a latent space of 32 dimensions. (see Sec. 4.4)

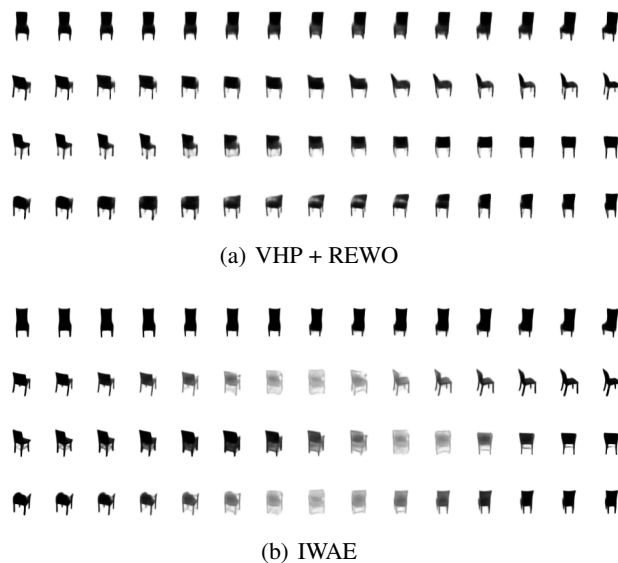


Figure 10. Chairs: interpolations along the learned latent manifold with a latent space of 32 dimensions. (see Sec. 4.4)

regression. The experiments on human motion data in Sec. 4.2 demonstrated that the learned hierarchical prior results in smoother interpolations compared to a standard prior and the VampPrior. This was also the case for the high-dimensional Faces and Chairs datasets (Sec. 4.4), leading to the conclusion that an informative representation of the data manifold was learned. Moreover, we obtained results comparable to state-of-art (test log-likelihood) on standard datasets, such as static and binary MNIST, Fashion-MNIST, and OMNIGLOT.

Acknowledgements

We would like to thank Maximilian Soelch for valuable suggestions and discussions.

References

- Alemi, A. A., Poole, B., Fischer, I., Dillon, J. V., Saurous, R. A., and Murphy, K. Fixing a broken ELBO. *ICML*, 2018.
- Aubry, M., Maturana, D., Efros, A. A., Russell, B. C., and Sivic, J. Seeing 3D chairs: exemplar part-based 2D-3D alignment using a large dataset of CAD models. *CVPR*, 2014.
- Bengio, Y., Lamblin, P., Popovici, D., and Larochelle, H. Greedy layer-wise training of deep networks. *NeurIPS*, 2007.
- Bowman, S. R., Vilnis, L., Vinyals, O., Dai, A., Jozefowicz, R., and Bengio, S. Generating sentences from a continuous space. *CoNLL*, 2016.
- Burda, Y., Grosse, R. B., and Salakhutdinov, R. Importance weighted autoencoders. *CoRR*, 2015.
- Cayton, L. Algorithms for manifold learning. *Univ. of California at San Diego Tech. Rep*, 12, 2005.
- Chen, N., Ferroni, F., Klushyn, A., Paraschos, A., Bayer, J., and van der Smagt, P. Fast approximate geodesics for deep generative models. *arXiv:1812.08284*, 2018.
- Chen, X., Duan, Y., Houthoofd, R., Schulman, J., Sutskever, I., and Abbeel, P. InfoGAN: Interpretable representation learning by information maximizing generative adversarial nets. *NeurIPS*, 2016a.
- Chen, X., Kingma, D. P., Salimans, T., Duan, Y., Dhariwal, P., Schulman, J., Sutskever, I., and Abbeel, P. Variational lossy autoencoder. *CoRR*, 2016b.
- Cremer, C., Morris, Q., and Duvenaud, D. Reinterpreting importance-weighted autoencoders. *arXiv:1704.02916*, 2017.
- Dilokthanakul, N., Mediano, P. A. M., Garnelo, M., Lee, M. C. H., Salimbeni, H., Arulkumaran, K., and Shanahan, M. Deep unsupervised clustering with gaussian mixture variational autoencoders. *CoRR*, 2016.
- Goyal, P., Hu, Z., Liang, X., Wang, C., and Xing, E. P. Nonparametric variational auto-encoders for hierarchical representation learning. *ICCV*, 2017.
- Higgins, I., Matthey, L., Pal, A., Burgess, C., Glorot, X., Botvinick, M., Mohamed, S., and Lerchner, A. Beta-VAE: Learning basic visual concepts with a constrained variational framework. *ICLR*, 2017.
- Kingma, D. P. and Welling, M. Auto-encoding variational bayes. *CoRR*, 2013.
- Lake, B. M., Salakhutdinov, R., and Tenenbaum, J. B. Human-level concept learning through probabilistic program induction. *Science*, 350, 2015.
- Larochelle, H. and Murray, I. The neural autoregressive distribution estimator. *AISTATS*, 2011.
- Lecun, Y., Bottou, L., Bengio, Y., and Haffner, P. Gradient-based learning applied to document recognition. *Proceedings of the IEEE*, 1998.
- Nalisnick, E. T. and Smyth, P. Stick-breaking variational autoencoders. *ICLR*, 2017.
- Neal, R. M. and Hinton, G. E. A view of the em algorithm that justifies incremental, sparse, and other variants. In *Learning in graphical models*. 1998.
- Paysan, P., Knothe, R., Amberg, B., Romdhani, S., and Vetter, T. A 3d face model for pose and illumination invariant face recognition. *AVSS*, 2009.
- Rezende, D. J. and Mohamed, S. Variational inference with normalizing flows. *ICML*, 2015.
- Rezende, D. J. and Viola, F. Taming VAEs. *arXiv:1810.00597*, 2018.
- Rezende, D. J., Mohamed, S., and Wierstra, D. Stochastic backpropagation and approximate inference in deep generative models. *ICML*, 2014.
- Rifai, S., Dauphin, Y. N., Vincent, P., Bengio, Y., and Muller, X. The manifold tangent classifier. *NeurIPS*, 2011.
- Sønderby, C. K., Raiko, T., Maaløe, L., Sønderby, S. K., and Winther, O. Ladder variational autoencoders. *NeurIPS*, 2016.
- Tomczak, J. and Welling, M. VAE with a VampPrior. *AISTATS*, 2018.
- Xiao, H., Rasul, K., and Vollgraf, R. Fashion-MNIST: a novel image dataset for benchmarking machine learning algorithms. *CoRR*, 2017.
- Yeung, S., Kannan, A., Dauphin, Y., and Fei-Fei, L. Tackling over-pruning in variational autoencoders. *CoRR*, 2017.
- Zhao, S., Song, J., and Ermon, S. Infovae: Information maximizing variational autoencoders. *CoRR*, 2017.

Appendix

A. β -Update Scheme in REWO and GECO

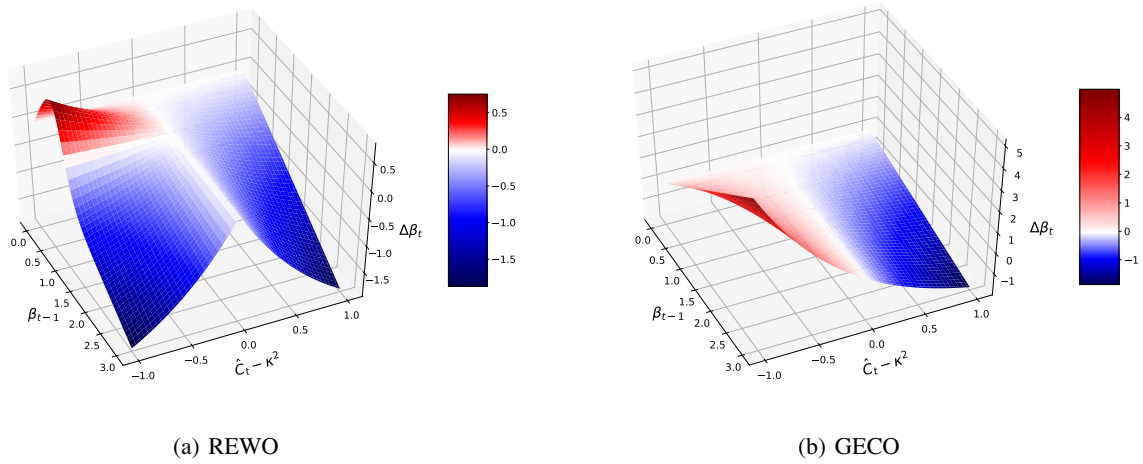


Figure 11. β -update scheme: $\Delta\beta_t = \beta_t - \beta_{t-1}$ as a function of β_{t-1} and $\hat{C}_t - \kappa^2$ for $\nu = 1$ and $\tau = 3$.

B. Pendulum

B.1. Training Process

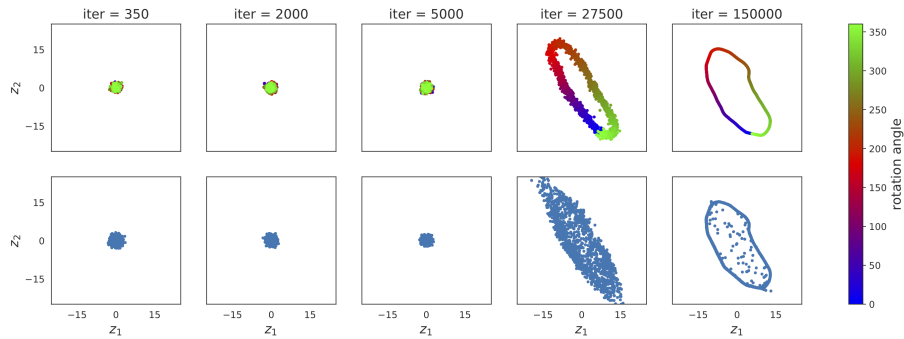


Figure 12. VHP (no REWO/GECO/WU): latent representation of the pendulum data at different iteration steps when optimising $\mathcal{L}_{\text{VHP}}(\theta, \phi, \Theta, \Phi; \beta = 1)$. The top row shows the approximate posterior, where the colour encodes the rotation angle of the pendulum. The bottom row shows samples from the hierarchical prior. It took 27,500 iterations until the model learned a representation of the data. However, the latent representation is less informative than in Fig. 2(a).

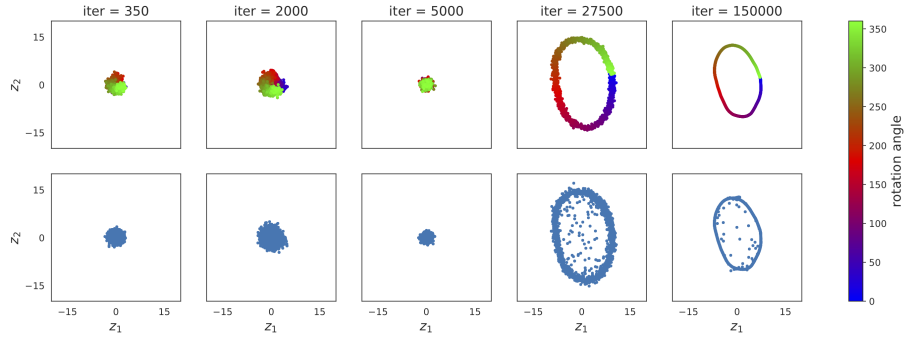


Figure 13. VHP + WU (20 epochs): latent representation of the pendulum data at different iteration steps when optimising $\mathcal{L}_{\text{VHP}}(\theta, \phi, \Theta, \Phi; \beta)$. The top row shows the approximate posterior, where the colour encodes the rotation angle of the pendulum. The bottom row shows samples from the hierarchical prior. The model started to learn a representation (iter=2000) but the fast increase β led to an over-regularisation by the KL term, resulting in a less informative representation than in Fig. 2(a).

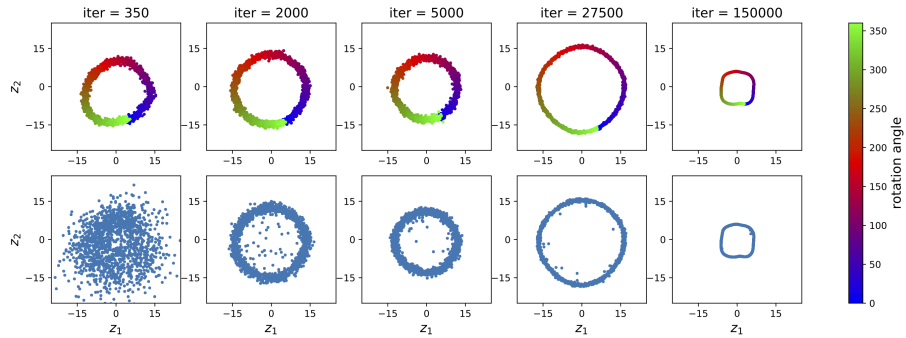


Figure 14. VHP + WU (200 epochs): latent representation of the pendulum data at different iteration steps when optimising $\mathcal{L}_{\text{VHP}}(\theta, \phi, \Theta, \Phi; \beta)$. The top row shows the approximate posterior, where the colour encodes the rotation angle of the pendulum. The bottom row shows samples from the hierarchical prior. The learned latent representation less informative than in Fig. 2(a).

B.2. OLS Regression on Learned Latent Representations

Fig. 15 shows the joint angle versus $\arcsin(z_2/r)$, where z_2 is the second component of the latent space and the radius r is estimated from the learned latent representation.

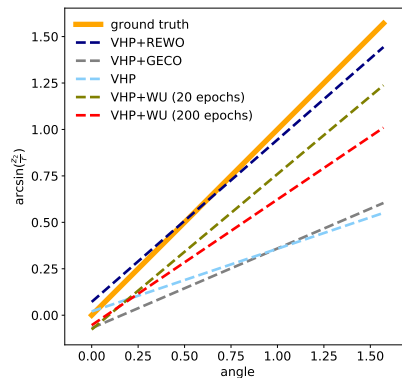


Figure 15. Verifying the learned latent representations of the VHP trained with REWO, GECO, or WU: OLS regressions on encodings of the pendulum data. The absolute errors are shown in Tab. 1.

B.3. VHP with ELBO instead of IW Bound

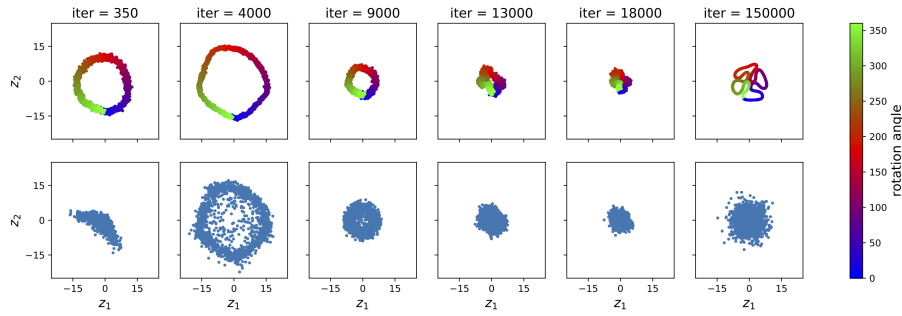


Figure 16. VHP + REWO (with ELBO instead of IW bound in the second stochastic layer): latent representation of the pendulum data at different iteration steps when optimising $\mathcal{L}_{\text{VHP}}(\theta, \phi, \Theta, \Phi; \beta)$. The top row shows the approximate posterior, where the colour encodes the rotation angle of the pendulum. The bottom row shows samples from the hierarchical prior.

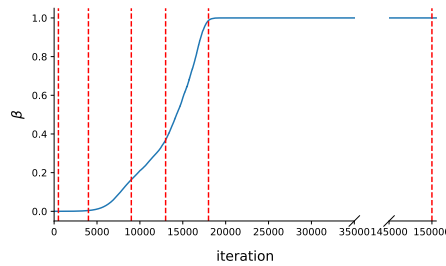


Figure 17. REWO: reconstruction-error-dependent increase of β . The red lines mark the respective iteration steps shown in Fig. 16. The model compensates the less expressive posterior $q_{\Phi}(\zeta|\mathbf{z})$ in the second stochastic layer by restricting $q_{\phi}(\mathbf{z}|\mathbf{x})$, which leads to poor latent representations.

B.4. Latent Representations Learned by VHP and IWAE

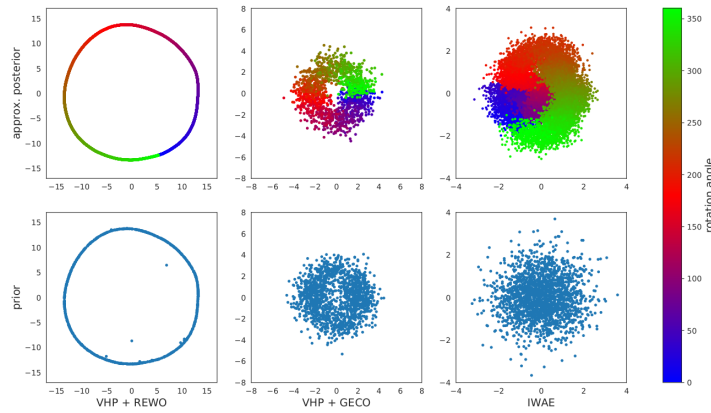
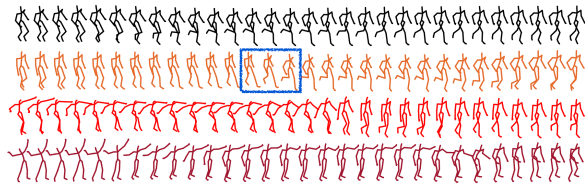
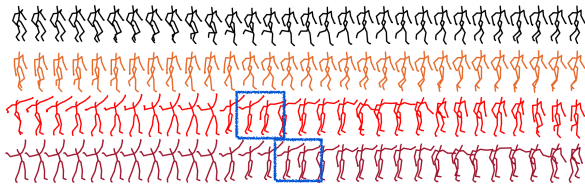


Figure 18. Latent representation of VHP + REWO (left), VHP + GECO (middle), and IWAE (right): approximate posterior (top) and prior (bottom). The colour encodes the rotation angle of the pendulum.

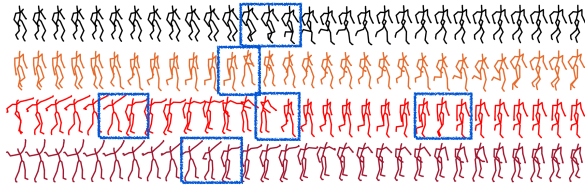
C. CMU Human Motion



(a) VHP + REWO



(b) VampPrior



(c) IWAE

Figure 19. Movement interpolation. The colour corresponds to Fig. 6. Discontinuities are marked by blue boxes.

D. Quantitative Results

D.1. Training Efficiency

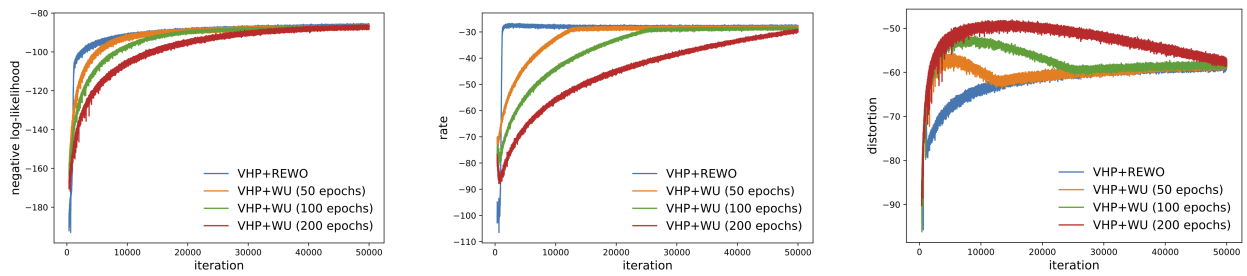
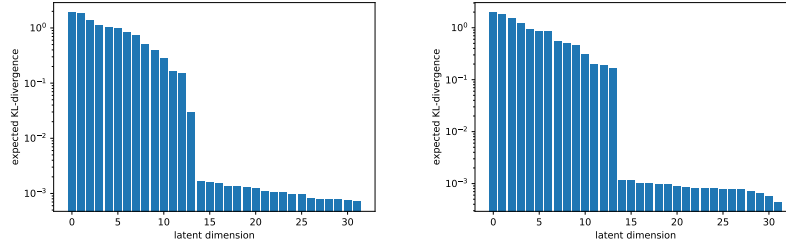


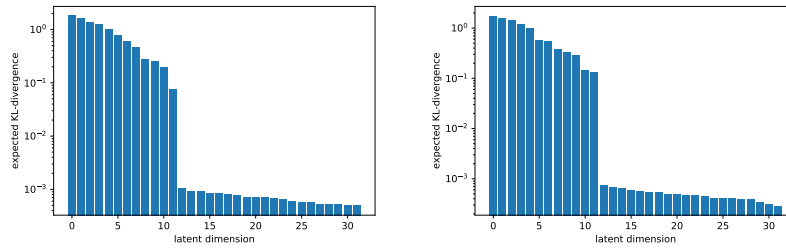
Figure 20. NLL vs rate vs distortion on static MNIST

D.2. Active Units

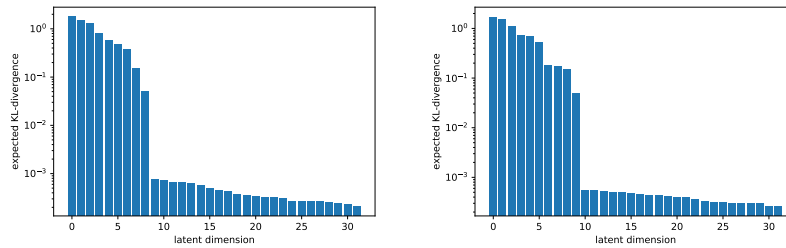
Furthermore, we evaluate whether REWO prevents over-pruning of the latent variables (Yeung et al., 2017). Following (Sønderby et al., 2016), we evaluate $KL(q_{\Phi}(\zeta^j|\mathbf{x}) || p(\zeta^j))$ for different optimisation strategies, where $\prod_j q_{\Phi}(\zeta^j|\mathbf{x}) = q_{\Phi}(\zeta|\mathbf{x})$. We show the results for the inner latent variable on several datasets in Fig. 21.



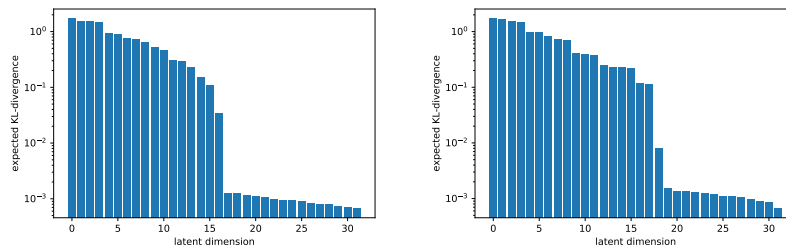
(a) static MNIST



(b) dynamic MNIST



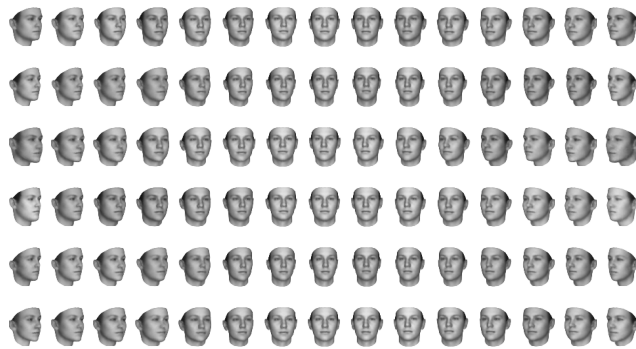
(c) Fashion-MNIST



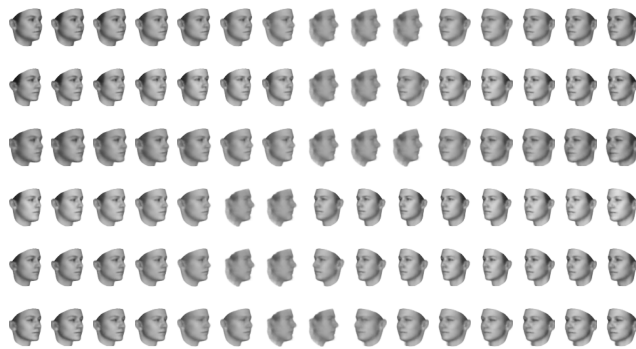
(d) OMNIGLOT

Figure 21. Expected KL divergence between approximate posterior and prior for REWO algorithm (left) and WU (right). The latent dimensions are sorted by the KL divergence and the histograms are shown on a logarithmic scale.

E. Faces and Chairs



(a) VHP + REWO

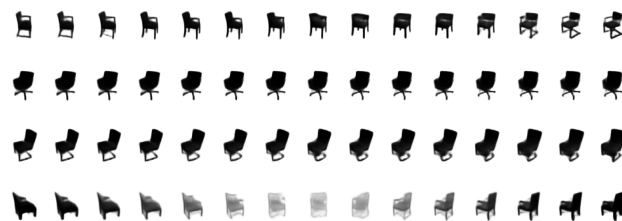


(b) IWAE

Figure 22. Faces: interpolations along the learned latent manifold with a latent space of 32 dimensions.



(a) VHP + REWO



(b) IWAE

Figure 23. Chairs: interpolations along the learned latent manifold with a latent space of 32 dimensions.

F. Model Architectures

Table 3. Model architectures. GatedFC/GatedConv denote pairs of fully-connected/convolutional layers multiplied element-wise, where one of the layers (gate) always uses sigmoid activations.

DATASET	OPTIMISER	ARCHITECTURE	
PENDULUM	ADAM $1e-4$	INPUT	256(FLATTENED 16×16)
		LATENTS	2
		$q_\phi(\mathbf{z} \mathbf{x})$	FC 256, 256, 256, 256. RELU ACTIVATION.
		$p_\theta(\mathbf{x} \mathbf{z})$	FC 256, 256, 256, 256. RELU ACTIVATION. GAUSSIAN.
		$q_\Phi(\zeta \mathbf{z})$	FC 256, 256, 256, 256, RELU ACTIVATION.
		$p_\Theta(\mathbf{z} \zeta)$	FC 256, 256, 256, 256, RELU ACTIVATION.
		OTHERS GRAPH	$\kappa = 0.02, \nu = 5, K = 16$. 1,000 NODES, 18 NEIGHBOURS.
CMU HUMAN	ADAM $1e-4$	INPUT	50
		LATENTS	2
		$q_\phi(\mathbf{z} \mathbf{x})$	FC 256, 256, 256, 256. RELU ACTIVATION.
		$p_\theta(\mathbf{x} \mathbf{z})$	FC 256, 256, 256, 256. RELU ACTIVATION. GAUSSIAN.
		$q_\Phi(\zeta \mathbf{z})$	FC 256, 256, 256, 256, RELU ACTIVATION.
		$p_\Theta(\mathbf{z} \zeta)$	FC 256, 256, 256, 256, RELU ACTIVATION.
		OTHERS GRAPH	$\kappa = 0.02, \nu = 1, K = 32$. 2,530 NODES, 15 NEIGHBOURS.
FACES, CHAIRS	ADAM $5e-4$	INPUT	$64 \times 64 \times 1$
		LATENTS	32
		$q_\phi(\mathbf{z} \mathbf{x})$	CONV $32 \times 5 \times 5$ (STRIDE 2), $32 \times 3 \times 3$ (STRIDE 1), $48 \times 5 \times 5$ (STRIDE 2). $48 \times 3 \times 3$ (STRIDE 1), $64 \times 5 \times 5$ (STRIDE 2), $64 \times 3 \times 3$ (STRIDE 1). $96 \times 5 \times 5$ (STRIDE 2), $96 \times 3 \times 3$ (STRIDE 1), FC 256. RELU ACTIVATION
		$p_\theta(\mathbf{x} \mathbf{z})$	DECONV REVERSE OF ENCODER. RELU ACTIVATION. BERNOULLI.
		$q_\Phi(\zeta \mathbf{z})$	FC 256, 256, RELU ACTIVATION.
		$p_\Theta(\mathbf{z} \zeta)$	FC 256, 256, RELU ACTIVATION.
		OTHERS GRAPH	$\kappa = 0.2, \nu = 1, K = 16$. 10,000 NODES (FACES), 8,637 NODES (CHAIRS), 18 NEIGHBOURS.
DYNAMICMNIST, STATICMNIST, FASHION-MNIST, OMNIGLOT	ADAM $5e-4$	INPUT	$28 \times 28 \times 1$
		LATENTS	32
		$q_\phi(\mathbf{z} \mathbf{x})$	GATEDCONV $32 \times 7 \times 7$ (STRIDE 1), $32 \times 3 \times 3$ (STRIDE 2), $64 \times 5 \times 5$ (STRIDE 1). $64 \times 3 \times 3$ (STRIDE 2), $6 \times 3 \times 3$ (STRIDE 1)
		$p_\theta(\mathbf{x} \mathbf{z})$	GATEDFC 784, GATEDCONV $64 \times 3 \times 3$ (STRIDE 1), $64 \times 3 \times 3$ (STRIDE 1), $64 \times 3 \times 3$ (STRIDE 1), $64 \times 3 \times 3$ (STRIDE 1). LINEAR ACTIVATION. BERNOULLI.
		$q_\Phi(\zeta \mathbf{z})$	GATEDFC 256, 256, LINEAR ACTIVATION.
		$p_\Theta(\mathbf{z} \zeta)$	GATEDFC 256, 256, LINEAR ACTIVATION.
		OTHERS OTHERS	$\kappa = 0.18$ (DYNAMICMNIST, STATICMNIST, OMNIGLOT), $\nu = 1, K = 16$. $\kappa = 0.31$ (FASHION-MNIST).